Since January 2020 Elsevier has created a COVID-19 resource centre with free information in English and Mandarin on the novel coronavirus COVID-19. The COVID-19 resource centre is hosted on Elsevier Connect, the company's public news and information website.

Chaos, Solitons and Fractals 107 (2018) 135–142

Contents lists available at ScienceDirect

Chaos, Solitons and Fractals

Nonlinear Science, and Nonequilibrium and Complex Phenomena

journal homepage: www.elsevier.com/locate/chaos

Multiple peaks patterns of epidemic spreading in multi-layer networks

Muhua Zheng[a], Wei Wang[b], Ming Tang[c], Jie Zhou[a], S. Boccaletti[d,e], Zonghua Liu[a,*]

[a] Department of Physics, East China Normal University, Shanghai 200241, China
[b] Web Sciences Center, University of Electronic Science and Technology of China, Chengdu 610054, China
[c] School of Information Science and Technology, East China Normal University, Shanghai 200241, China
[d] CNR-Institute of Complex Systems, Via Madonna del Piano, 10, 50019 Sesto Fiorentino, Florence, Italy
[e] The Embassy of Italy in Tel Aviv, 25 Hamered Street, 68125 Tel Aviv, Israel

ARTICLE INFO

Article history:
Received 29 November 2017
Accepted 25 December 2017
Available online 3 January 2018

Keywords:
Epidemic spreading
multi-layer networks
Multiple peaks patterns
Complex networks

ABSTRACT

The study of epidemic spreading on populations of networked individuals has seen recently a great deal of significant progresses. A common point in many of past studies is, however, that there is only one peak of infected density in each single epidemic spreading episode. At variance, real data from different cities over the world suggest that, besides a major single peak trait of infected density, a finite probability exists for a pattern made of two (or multiple) peaks. We show that such a latter feature is distinctive of a multilayered network of interactions, and reveal that a two peaks pattern may emerge from different time delays at which the epidemic spreads in between the two layers. Further, we show that the essential ingredient is a weak coupling condition between the layers themselves, while different degree distributions in the two layers are also helpful. Moreover, an edge-based theory is developed which fully explains all numerical results. Our findings may therefore be of significance for protecting secondary disasters of epidemics, which are definitely undesired in real life.

1. Introduction

Epidemic spreading in networked populations has been studied intensely in the last decade, and a lot of great progresses has been achieved [1–4] which significantly increased our understanding. This is actually useful for public health authorities to assess situations quickly, to take and enforce informed decisions, and to optimize vaccination and drug delivery policies. Initially, the main attention focused on static networks, where each node represents an immobile agent and the contagion occurs only between neighboring nodes: it was revealed that scale-free networks display a vanishingly small epidemic threshold in the thermodynamic limit [5,6]. After that, the focus shifted to reaction-diffusion models [7–10], flow-driven epidemics [11–15], objective spreading [16,17] and adaptive behaviors [18–22]. Finally, in a third stage, multilayered [23–32] and temporal [33,34] networks were assumed to play a critical role on such processes.

A common feature in past studies is the use of phenomenological models which typically produce a single peak of infected density in each individual epidemic spreading. An interesting question is therefore whether or not all real evolutionary processes are conveniently represented by such a framework. A scrupulous analysis of a large number of real data from different cities over the world surprisingly shows that, besides a major pattern made of a single peak, there is a finite and non negligible probability for a new pattern of epidemic outbreak featuring two (or multiple) peaks. Notice that a two peaks pattern implies two outbreaks in a single spreading period, i.e. a secondary occurrence of the same epidemics, which may in turn produce severe calamities and disasters within unprepared populations. Understanding the underlying mechanism at the basis of this new pattern (with the help of a novel model extracted from real data) is therefore quintessential to properly cope with such life-threatening hazards. Previous studies showed that the phenomenon of multiple peaks in epidemics may occur in weak coupled different communities, where a full homogeneous mixing cannot be assumed [35–38]. Considering that human behaviors occur in social networks, a key problem for further studies is how the network structures influence the formation of two-peaks patterns and the transition between the case of single peak and that of two peaks.

We here study this problem by presenting a network based model to reproduce the phenomenon of two peaks from epidemic data. As social activities and interactions occur in network structures, we here consider the epidemics in different geographic regions (or cities) as that occurring in multilayered graphs. Namely, we will take two coupled neighboring regions as an example, and construct a two-layered network model which fully reproduces the

* Corresponding author.
E-mail address: zhliu@phy.ecnu.edu.cn (Z. Liu).

https://doi.org/10.1016/j.chaos.2017.12.026
0960-0779/

observed patterns of epidemics. In particular, we demonstrate that the pattern of two peaks originates from large time delays of epidemic outbreaks between the two layers, which depends in turn on both the difference in the degree distributions of the two layers and a weak coupling condition between them. To better understand the findings, an edge-based theory is developed which perfectly agree with the numerical simulations.

2. Patterns of epidemic outbreak with two or multiple peaks in real data

Monitoring the potential outbreaks of an epidemic spreading is of extreme importance for protection of our society. Based on the detected trend of spreading of infections such as SARS (Severe Acute Respiratory Syndrome), H1N1 (Swine Influenza), H5H1 (Avian Influenza), and Ebola, one can indeed attempt to enforce suitable measures able to reduce the epidemic at its maximum extent. For this purpose, many countries have established their sentinel surveillance systems to collect epidemic data. For instance, Hong Kong Department of Health has organized a surveillance system, with the aim of collecting empirical data of infectious diseases, and of analyzing and predicting the trend of the infection. In such a system, there are about 64 General Out-Patient Clinics (GOPC) and 50 General Practitioners (GP), which form two distinct sentinel surveillance networks of the city [39,40]. In these two networks, one obtains for instance the weekly consultation rates of influenza-like illness (per 1,000 consultations), which reflect the overall influenza-like illness activity in Hong Kong.

Fig. 1(a) shows the collected data from 1998/1/3 to 2014/8/2 in GP, while the corresponding data of GOPC is not shown here. From Fig. 1(a) one sees that there are many events of epidemic spreading, and the intervals between two consecutive events are not regular, indicating non-periodic outbreaks of recurrent epidemics [40]. On the other hand, one notices from Fig. 1(a) that most of the outbreaks correspond to a single peak of infected density, which is the pattern well described by the classical susceptible-infected-refractory (SIR) models. However, one notices also that there is a finite probability for a novel pattern of epidemic outbreak which features, instead, two or multiple peaks. Fig. 1(b) shows one of such patterns (with two peaks) occurring at around 2005/6, which indicates that an infectious disease raised two times during that epidemic period in Hong Kong. Such unexpected phenomenon also exists in the data from GOPC (not shown here).

These multiple peaks patterns are actually occurring generically, and are not limited to a specific geographical region. Epidemic data from other sources and cities display, indeed, ubiquitously patterns similar to that reported in Fig. 1(b). For instance, Fig. 1(c) shows the data of the weekly measles infective cases (WMICs) from 1908 to 1937 in Boston [41,42], and a two peaks pattern is shown in Fig. 1(d) at around 1915/4. In addition, two or multiple peaks of infected density may characterize the outbreaks in the total number of WMICs of two neighboring cities, also when uni-modal patterns are actually observed in each individual city. For example, Fig. 1(e) and (f) report the data of WMICs in Bristol and Newcastle [43]: the yellow line denotes the total number of WMICs, whereas the blue and green lines represent the data in Bristol and Newcastle, respectively. In Fig. 1(f) one can well appreciate that the pattern of two peaks occurs only in the total number of WMICs. Similarly, Fig. 1(g) and (h) show the case of Bristol and Sheffield [43], and once again a typical two peaks pattern [Fig. 1(h)] occurs.

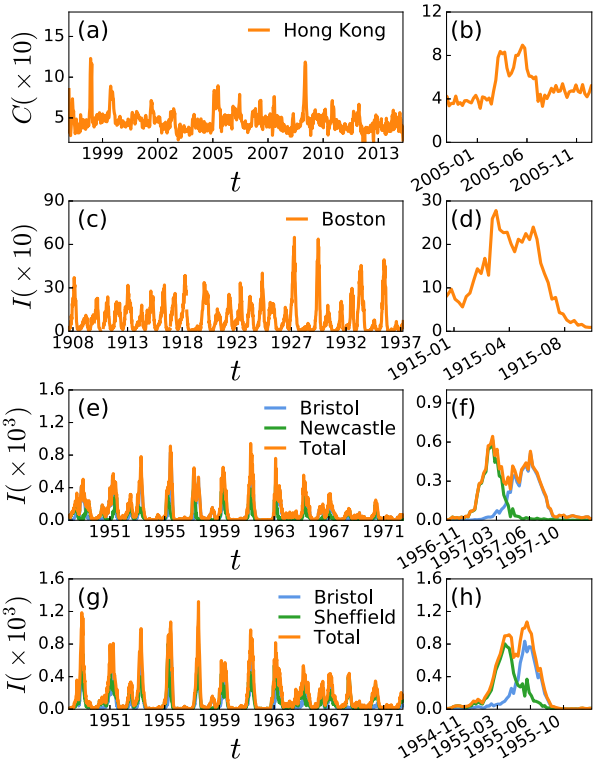

Fig. 1. Time series of recurrent epidemics in different cities over the world. (a) The weekly consultation rates of influenza-like illness (per 1000 consultations) from 1998/1/3 to 2014/8/2 in Hong Kong for the General Practitioners (GP) sentinel system. (b) Zoom of one of the patterns with two peaks, occurring at around 2005/6 in (a). (c) The time series of reported weekly measles infective cases I in Boston. (d) Zoom of one of the patterns with two peaks, occurring at around 1915/4 in (c). (e)–(h): Time series of infectious disease in two coupled cities. (e) and (f): The yellow line represents the total number of weekly measles infective cases in coupled Bristol and Newcastle, while the blue and green lines represent the number in Bristol and Newcastle, respectively. (f) is one of the patterns, occurring at around 1957/3 in (e). (g) and (h): The yellow line represents the total number of weekly measles infective cases in coupled Bristol and Sheffield, while the blue and green lines represent the number in Bristol and Sheffield, respectively. (h) is one of the patterns, occurring at around 1955/5 in (g). (For interpretation of the references to color in this figure legend, the reader is referred to the web version of this article.)

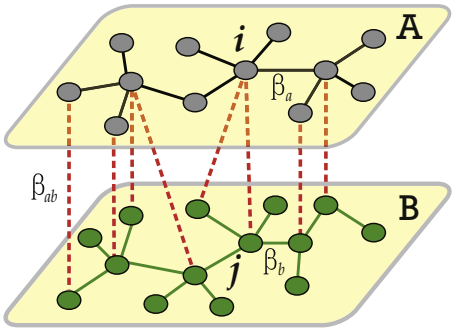

Fig. 2. Sketch of the two-layered network model, which reproduces the pattern of two peaks. "Black", "green" and "red" lines represent the links of the networks $\mathcal{A}$, $\mathcal{B}$ and the inter-network $\mathcal{AB}$, respectively. β_a, β_b and β_{ab} denote the infectious rates of networks $\mathcal{A}$, $\mathcal{B}$ and $\mathcal{AB}$. (For interpretation of the references to color in this figure legend, the reader is referred to the web version of this article.)

3. The two-layered network model

To capture the underlying mechanism, we introduce a model of a two-layered network, where the two layers represent actually two interconnected regions or cities. Fig. 2 is a sketch of the model: $\mathcal{A}$ and $\mathcal{B}$ are the two layers, which are coupled through the inter-network $\mathcal{AB}$. For the sake of simplicity, we let the two networks $\mathcal{A}$ and $\mathcal{B}$ have the same size $N_a = N_b$. Furthermore, $\langle k_a \rangle$, $\langle k_b \rangle$, and $\langle k_{ab} \rangle$ represent the average degrees of networks $\mathcal{A}$, $\mathcal{B}$ and $\mathcal{AB}$, respectively. In details, we first generate two separated networks $\mathcal{A}$ and $\mathcal{B}$ with the same size N and different degree distributions $P_A(k)$

and $P_B(k)$, respectively. Then, we add links between $\mathcal{A}$ and $\mathcal{B}$. That is, we randomly choose two nodes from $\mathcal{A}$ and $\mathcal{B}$ and then connect them if they are not connected yet. The process is repeated until all the needed specifications are attained. In the above way, one obtains a uncorrelated two-layered network.

Under such a framework, we adopt the Susceptible-Infected-Refractory (SIR) model to study the epidemic spreading dynamics. Particularly, each node is a unit of the SIR model, where *S, I* and *R* represent the susceptible, infected and refractory phases of individuals, respectively. At each time step, a susceptible node will be infected by an infected neighbor with rate β, and an infected node will become refractory with probability μ. The infectious process will be considered terminated when no more infected nodes exist. While μ is taken to be the same for all networks, we let β_a, β_b and β_{ab} be the infectious rates of networks $\mathcal{A}$, $\mathcal{B}$ and $\mathcal{AB}$, respectively. Thus, a susceptible node will be infected with a probability $1-(1-\beta_a)^{k^{inf}}(1-\beta_{ab})^{k_{ab}^{inf}}$, where k^{inf} is the infected neighbors in the same network and k_{ab}^{inf} is the infected neighbors in the coupled network.

In our numerical simulations, we choose $\mathcal{A}$ to be a scale-free (SF) network with degree distribution $P_A(k)\sim k^{-\gamma}$ [44], and $\mathcal{B}$ a random regular (RR) network with a constant degree k_b [45]. The network size is $N_a = N_b = 10\,000$, the average degree $\langle k_a\rangle = \langle k_b\rangle = 6$, and initially 0.1% of individuals of network $\mathcal{A}$ are chosen to be infected.

4. Results

4.1. The two peaks outbreak pattern in simulations

A pattern of two peaks appears in the numerical simulations of our model. The yellow circles in Fig. 3(a) report the evolution of the infected density ρ_I in the whole network with the parameters $\gamma = 2.1$, $\langle k_a\rangle = \langle k_b\rangle = 6$, $\langle k_{ab}\rangle = 1.0$, $\beta_a = \beta_b = 0.05$, $\beta_{ab} = 0.005$ and $\mu = 0.1$. One can easily differentiate two peaks of ρ_I, indicating that the empirical observations in Fig. 1 can be fully reproduced.

To gather a deeper understanding, we also measure the evolutions of ρ_I^A and ρ_I^B in both layers $\mathcal{A}$ and $\mathcal{B}$, and report them as green triangles and blue squares in Fig. 3(a), respectively. It is easy to see that the times at which the maximum infected density is obtained in layers $\mathcal{A}$ and $\mathcal{B}$ are different, implying that the pattern of two peaks is likely triggered by the time difference of epidemic outbreaks in the two layers.

4.2. The factors determining the occurrence of two peaks pattern

The next step is to focus on the factors that determines the occurrence of such two peaks pattern. For this purpose, we first concentrate on the role of the average degree $\langle k_{ab}\rangle$ of the inter-network $\mathcal{AB}$. Fig. 3(b) shows the evolution of the infected density ρ_I with different $\langle k_{ab}\rangle$ (with triangles, squares and circles denoting the cases of $\langle k_{ab}\rangle = 3.0, 1.0$ and 0.5, respectively). One notices that the pattern of ρ_I is uni-modal when $\langle k_{ab}\rangle$ is large, but bi-modal when $\langle k_{ab}\rangle$ is sufficiently small, indicating that $\langle k_{ab}\rangle$ is a key factor for the appearance of a bimodal pattern: a smaller $\langle k_{ab}\rangle$ favours the appearance of the two peaks pattern, indicating that the two main networks $\mathcal{A}$ and $\mathcal{B}$ should be only weakly coupled among them.

Further, we study the influence of the infectious rate β_{ab} on the pattern. Fig. 3(c) reports the results obtained for different β_{ab} (with triangles, squares and circles representing the cases of $\beta_{ab} = 0.05, 0.005$ and 0.001, respectively). Once again one may notice that the condition of a weak coupling is essential for a bimodal pattern: ρ_I is indeed uni-modal when β_{ab} is large, while

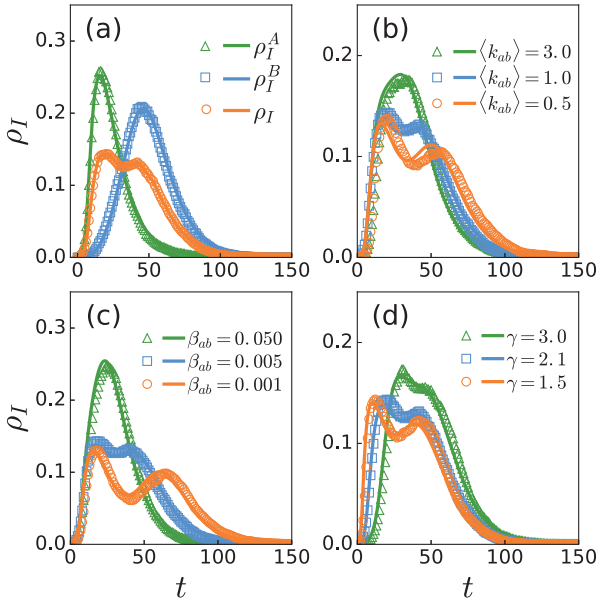

Fig. 3. The two peaks pattern occurring in different conditions, with $\mu = 0.1$, $\beta_a = \beta_b = 0.05$, $\langle k_a\rangle = \langle k_b\rangle = 6$, and $N_a = N_b = 10,000$, where the symbols represent the simulated results and the lines denote the corresponding theoretical predictions (calculated via the edge-based compartmental theory described in the Method section). (a) $\rho_I(t)$ vs. t, where ρ_I, ρ_I^A and ρ_I^B represent the infected densities in the entire network, and the networks $\mathcal{A}$ and $\mathcal{B}$, respectively. Other parameters are $\gamma = 2.1$, $\langle k_{ab}\rangle = 1.0$, and $\beta_{ab} = 0.005$. (b) The influence of $\langle k_{ab}\rangle$ on $\rho_I(t)$ with $\gamma = 2.1$ and $\beta_{ab} = 0.005$, where the "triangles", "squares" and "circles" represent the cases of $\langle k_{ab}\rangle = 3.0, 1.0$ and 0.5, respectively. (c) The influence of β_{ab} on $\rho_I(t)$ with $\gamma = 2.1$ and $\langle k_{ab}\rangle = 1.0$, where the "triangles", "squares" and "circles" represent the cases of $\beta_{ab} = 0.05, 0.005$ and 0.001, respectively. (d) The influence of γ on $\rho_I(t)$ with $\beta_{ab} = 0.005$ and $\langle k_{ab}\rangle = 1.0$, where the "triangles", "squares" and "circles" represent the cases of $\gamma = 3.0, 2.1$ and 1.5, respectively.

the two peaks appear when β_{ab} is small. Finally, we study the influence of the exponent γ of the SF network. Fig. 3(d) shows that the bimodal feature is reduced with the increase of γ. As a larger γ means a smaller difference between the structures of the SF and RR networks, one can infer that the heterogeneity between the two layers is very helpful for the appearance of two peaks patterns.

All the numerical results are fully confirmed by an edge-based compartmental theory, see our theoretical Eqs. (18) and (19) in the *Theoretical analysis* section. The solid curves in Fig. 3(a)–(d) show the corresponding theoretical results.

These numerics point that a weak coupling is the necessary condition for the emergence of the new pattern, while a difference in heterogeneity between the two layers is a very helpful factor. An interesting question is whether the observed behavior corresponds to a critical phenomenon. To figure out the answer, we let τ be the time interval between the two peaks of ρ_I. In particular, the two peaks will merge into a single one when $\tau = 0$. Similarly, we let $\delta_t = \mid t_{max}^B - t_{max}^A \mid$ be the time delay between the two peaks in layers $\mathcal{A}$ and $\mathcal{B}$, where t_{max}^A and t_{max}^B are the times of occurrence of the peak in ρ_I^A and ρ_I^B, respectively. The trivial situation would be that for which $\tau = \delta_t$, but our numerical simulations show that this condition is attained only when τ is large, whereas one has $\tau < \delta_t$ when τ is sufficiently small. And, in particular, one has $\delta_t > 0$ when $\tau = 0$.

Fig. 4(a) and (b) show the dependence of τ and δ_t on β_{ab} for fixed $\gamma = 2.1$ and different $\langle k_{ab}\rangle$, respectively. From Fig. 4(a), one sees that when $\langle k_{ab}\rangle$ is small, τ will decrease monotonically and be non-vanishing with the increasing of β_{ab}, indicating that the event of two peaks always exists in the pattern. However, when $\langle k_{ab}\rangle$ is increased, τ will decrease rapidly to zero, implying that there is a critical β_{ab}^c for different $\langle k_{ab}\rangle$. When $\beta_{ab} < \beta_{ab}^c$, the epidemic

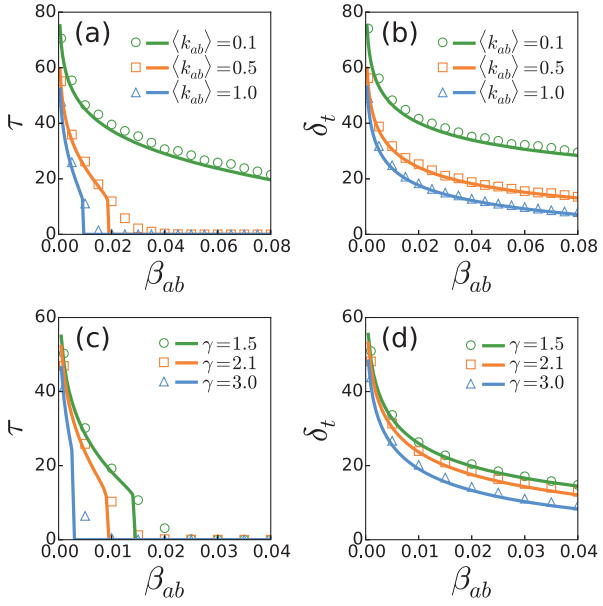

Fig. 4. (a) and (b) report the dependence of τ and δ_t on β_{ab} (see main text for definitions) with different $\langle k_{ab}\rangle$ in SF-RR networks. (c) and (b) report the dependence of τ and δ_t on β_{ab} with different γ in SF-RR networks. Symbols represent the simulated results and the lines are the corresponding theoretical results (calculated via the edge-based compartmental theory described in the Method section). Other parameters as in the caption of Fig. 3. All the results are averaged over 100 independent realizations.

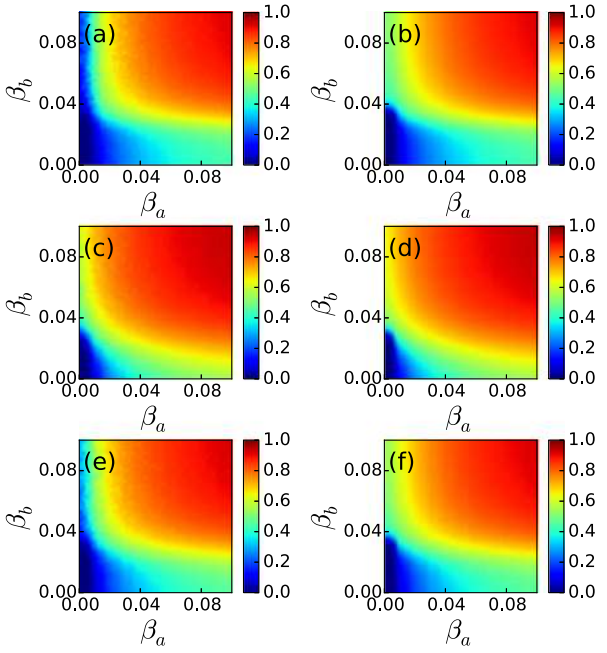

Fig. 5. Dependence of the final epidemic size ρ_R on β_a and β_b in SF-RR networks with $\langle k_{ab}\rangle = 1.0$ and $\beta_{ab} = 0.005$ in (a)-(b), $\langle k_{ab}\rangle = 1.0$ and $\beta_{ab} = 0.05$ in (c)-(d), and $\langle k_{ab}\rangle = 2.0$ and $\beta_{ab} = 0.005$ in (e)-(f). Left and right panels correspond to numerical simulations and theoretical results, respectively. All the numerical results are averaged over 100 independent realizations. Other parameters are set as $P_A(k) \sim k^{-\gamma}$, $\gamma = 2.1$, $\langle k_a\rangle = 6$, $\langle k_b\rangle = 6$, $\mu = 0.1$ and $N_a = N_b = 10,000$.

spreading event occurs through a pattern of two peaks in the infected density, while for $\beta_{ab} > \beta_{ab}^c$ it occurs via the traditional pattern with a single peak. On its turn, Fig. 4(b) shows that δ_t decreases monotonically with the increase of β_{ab} for all the three cases of $\langle k_{ab}\rangle$, and it never vanishes. This is because the spreading speed is different in homogeneous and heterogeneous networks. Generally speaking, epidemic spreading is faster in heterogeneous network than in homogeneous network [46].

We then turn to investigate the influence of the heterogeneity in degree distribution on the occurrence of the two peaks pattern. Fig. 4(c) and (d) show the dependence of τ and δ_t on β_{ab} for different γ and fixed $\langle k_{ab}\rangle = 1.0$. While the network heterogeneity decreases with the increasing of γ, it is easy to see that when γ is large, τ and δ_t decrease more prominently with β_{ab}. Specifically, the difference of spreading speeds between the two layers is not distinctive for large γ, resulting in the disappearance of the two peaks. Therefore, increasing the coupling strength (i.e. $\langle k_{ab}\rangle$ and β_{ab}) or decreasing the heterogeneity of network topology between the networks $\mathcal{A}$ and $\mathcal{B}$ will decrease the time delay of epidemic outbreak and then suppress the pattern of two peaks.

We have also confirmed all these numerical results in Fig. 4(a)–(d) by the theoretical Eqs. (18) and (19) in the *Theoretical analysis* section. For each set of parameters in Fig. 4(a)–(d), we first produce the infected densities ρ_I, ρ_I^A, and ρ_I^B from Eqs. (18) and (19), as done in Fig. 3(a)–(d), and then measure the corresponding τ and δ_t. The solid curves in Fig. 4(a)–(d) show the theoretical τ and δ_t. One can easily see that the theoretical results are fully consistent with the numerical results.

4.3. The effect of the coupling strength on the final epidemic size

In the above text, we have discussed that the value of the coupling strength is crucial for determining the kind of pattern of the epidemic spreading. Then, a natural question is how the coupling strength influences the final size of epidemic spreading. Fig. 5 shows the dependence of the final value of ρ_R on β_a and β_b for a scale-free (SF)-random regular (RR) network configuration, with different $\langle k_{ab}\rangle$ and β_{ab}. All the results are averaged over 100 independent realizations with $\langle k_{ab}\rangle = 1.0$ and $\beta_{ab} = 0.005$ in (a), $\langle k_{ab}\rangle = 1.0$ and $\beta_{ab} = 0.05$ in (c), and $\langle k_{ab}\rangle = 2.0$ and $\beta_{ab} = 0.005$ in (e), respectively. Comparing Fig. 5(a) with (c), one sees that the blue area in (c) is much smaller than that in (a), indicating that increasing β_{ab} has the effect of enhancing the final epidemic size. Comparing Fig. 5(a) with (e), one sees that the blue area in (e) is slightly smaller than that in (a), indicating that increasing $\langle k_{ab}\rangle$ can also slightly enhance ρ_R.

On the other hand, one can also obtain ρ_R by the theoretical formulae in the theoretical analysis Section. The right panels in Fig. 5 (i.e. Fig. 5(b), (d) and (f)) show the results corresponding to the left panels, respectively, and indicate that all theoretical predictions are highly consistent.

5. Theoretical analysis

5.1. Edge-based compartmental theory for a single network

Let us first illustrate the edge-based compartmental theory for a single network, by following the methods and tools introduced in Refs. [47–56].

For an uncorrelated, large and sparse network, the SIR model can be described in terms of the quantities $S(t)$, $I(t)$, and $R(t)$, which represent the densities of the susceptible, infected, and recovered nodes at time t, respectively. Let $\theta(t)$ be the probability that a neighbor v of u has not transmitted the disease to u along the edge connecting them up to time t. Then, the node u with degree k is susceptible at time t as $s(k,t) = \theta(t)^k$. Averaging over all k, the density of susceptible nodes at time t is given by

$$S(t) = \sum_{k=0}^{\infty} P(k)\theta(t)^k \tag{1}$$

where $P(k)$ is the degree distribution of the network. In order to solve for $S(t)$, one needs to know $\theta(t)$. Since a neighbor v of node u may be susceptible, infected, or recovered, $\theta(t)$ can be expressed as

$$\theta(t) = \Phi^S(t) + \Phi^I(t) + \Phi^R(t) \tag{2}$$

where $\Phi^S(t)$, $\Phi^I(t)$, $\Phi^R(t)$ is the probability that the neighbor v is in the susceptible, infected, recovery state, respectively, and has not transmitted the disease to node u through their connection. Once these three parameters can be derived, we will get the density of susceptible nodes at time t by substituting them into Eq. (2) and then into Eq. (1). To this purpose, in the following, we will focus on how to solve them.

To find $\Phi^S(t)$, we now consider a randomly chosen node u, and assume this node is in the cavity state, which means that it cannot transmit any disease to its neighbors v but can be infected by its neighbors. In this case, the neighbor v can only get the disease from its other neighbors except the node u. Thus, node v with degree k' is susceptible with probability $\theta(t)^{k'-1}$ at time t. For uncorrelated networks, the probability that one edge from node u connects with a node v with degree k' is $k'P(k')/\langle k\rangle$. Summing over all possible k', one obtains

$$\Phi^S(t) = \frac{\sum_{k'} k'P(k')\theta(t)^{k'-1}}{\langle k\rangle} \tag{3}$$

According to the SIR spreading process, the growth of $\Phi^R(t)$ includes two consecutive events: first, an infected neighbor has not transmitted the infection to node u via with probability $1-\beta$; second, the infected neighbor has been recovered with probability μ. Combining these two events, the $\Phi^I(t)$ to $\Phi^R(t)$ flux is $\mu(1-\beta)\Phi^I(t)$. Thus, one gets

$$\frac{d\Phi^R(t)}{dt} = \mu(1-\beta)\Phi^I(t) \tag{4}$$

Once the infected neighbor v transmits the disease to u successfully (with probability β), the $\Phi^I(t)$ to $1-\theta(t)$ flux will be $\beta\Phi^I(t)$, which means

$$\frac{d(1-\theta(t))}{dt} = \beta\Phi^I(t)$$

That is

$$\frac{d\theta(t)}{dt} = -\beta\Phi^I(t) \tag{5}$$

Combining Eqs. (4) and (5), and considering (as initial conditions) $\theta(0)=1$ and $\Phi^R(0)=0$, one obtains

$$\Phi^R(t) = \frac{\mu(1-\theta(t))(1-\beta)}{\beta} \tag{6}$$

Substituting Eqs. (3) and (6) into Eq. (2), one gets an expression for $\Phi^I(t)$ in terms of $\theta(t)$, and then one can rewrite Eq. (5) as

$$\begin{aligned}\frac{d\theta(t)}{dt} &= -\beta\theta(t) + \beta\frac{\sum_{k'} k'P(k')\theta(t)^{k'-1}}{\langle k\rangle} \\ &\quad +\mu(1-\theta(t))(1-\beta)\end{aligned} \tag{7}$$

After obtaining the solution of Eq. (7), we can substitute it into Eq. (1) to obtain $S(t)$. Then, $I(t)$ and $R(t)$ can be obtained as follows

$$\frac{dR(t)}{dt} = \mu I(t), \quad I(t) = 1 - S(t) - R(t) \tag{8}$$

In fact, Eq. (7) does not depend on Eq. (8), so the system is governed by the single ordinary differential equation (7). Although the resulting equation are simpler than those found by other methods, it can be proven to exactly predict the disease dynamics in the large-population limit for different network topologies [53,57].

5.2. The theory for two-layered networks

When one assumes that the population is made up of two interacting networks, then $P_j(k_1, k_2)$ denote the probability that a node of network j has k_1 degree in network 1 and k_2 in network 2. For the sake of simplicity, one can name the two networks $\mathcal{A}$ and $\mathcal{B}$ as 1 and 2. Let $\beta_{j,l}$ be the rate of transmission across an edge from network l to network j, and let us define μ to be the recovery rate of a node in any network.

$\theta_{j,l}$ can be defined to be the probability that an edge to a test node u in network j ($j=1,2$) is coming from network l ($l=1,2$), and has not transmitted the infection.

Now, $\theta_{1,2}$ can be solved as in the case of a single network. Since a neighbor v in network 2 of node u in network 1 may be susceptible, infected, or recovered, $\theta_{1,2}$ can be expressed as

$$\theta_{1,2} = \Phi^S_{1,2} + \Phi^I_{1,2} + \Phi^R_{1,2} \tag{9}$$

where $\Phi^S_{1,2}$, $\Phi^I_{1,2}$, $\Phi^R_{1,2}$ is the probability that the neighbor v is in the susceptible, infected, recovery state, and has not transmitted the disease to node u through their connection.

Similarly, to find $\Phi^S_{1,2}$, the neighbor v in network 1 can only get the disease from its other neighbors except the node u in network 2. Thus, the node v with degree k_1 in network 1 and degree k_2 in network 2 is susceptible with probability $\theta_{2,1}^{k_1-1}\theta_{2,2}^{k_2}$ at time t. For uncorrelated networks, the probability that one edge from node u connects with a node v with degree (k_1, k_2) is $\frac{k_1P_2(k_1,k_2)}{\sum_{k_1,k_2}k_1P_2(k_1,k_2)}$. Thus, one has

$$\Phi^S_{1,2} = \frac{\sum_{k_1,k_2} k_1P_2(k_1,k_2)\theta_{2,1}^{k_1-1}\theta_{2,2}^{k_2}}{\sum_{k_1,k_2} k_1P_2(k_1,k_2)} \tag{10}$$

It is easily to know that the growth of $\Phi^R_{1,2}$ includes two consecutive events: first, an infected neighbor has not transmitted the infection to node u via with probability $1-\theta_{1,2}$; second, the infected neighbor has been recovered with probability μ. Combining these two events, the $\Phi^I_{1,2}$ to $\Phi^R_{1,2}$ flux is $\mu(1-\theta_{1,2})\Phi^I_{1,2}$. Thus, one gets

$$\frac{d\Phi^R_{1,2}}{dt} = \mu(1-\theta_{1,2})\Phi^I_{1,2} \tag{11}$$

Once the infected neighbor v in network 1 transmits the disease to node u in network 2 successfully (with probability $\beta_{1,2}$), the $\Phi^I_{1,2}$ to $1-\theta_{1,2}$ flux will be $\beta_{1,2}\Phi^I_{1,2}$, which means

$$\frac{d\theta_{1,2}}{dt} = -\beta_{1,2}\Phi^I_{1,2} \tag{12}$$

Combining Eqs. (11) and (12), and considering (as initial conditions) $\theta_{1,2}(0)=1$ and $\Phi^R_{1,2}(0)=0$, one obtains

$$\Phi^R_{1,2} = \frac{\mu(1-\theta_{1,2})(1-\beta_{1,2})}{\beta_{1,2}} \tag{13}$$

So, one gets

$$\begin{aligned}\dot\theta_{1,2} &= -\beta_{1,2}(\theta_{1,2} - \Phi^S_{1,2} - \Phi^R_{1,2}) \\ &= -\beta_{1,2}\theta_{1,2} + \beta_{1,2}\frac{\sum_{k_1,k_2} k_1P_2(k_1,k_2)\theta_{2,1}^{k_1-1}\theta_{2,2}^{k_2}}{\sum_{k_1,k_2} k_1P_2(k_1,k_2)} \\ &\quad +\mu(1-\theta_{1,2})(1-\beta_{1,2})\end{aligned} \tag{14}$$

Similarly, one can write down $\theta_{1,1}$, $\theta_{2,1}$ and $\theta_{2,2}$ as follows

$$\begin{aligned}\dot\theta_{1,1} &= -\beta_{1,1}\theta_{1,1} + \beta_{1,1}\frac{\sum_{k_1,k_2} k_1P_1(k_1,k_2)\theta_{1,1}^{k_1-1}\theta_{1,2}^{k_2}}{\sum_{k_1,k_2} k_1P_1(k_1,k_2)} \\ &\quad +\mu(1-\theta_{1,1})(1-\beta_{1,1})\end{aligned} \tag{15}$$

$$\dot{\theta}_{2,1} = -\beta_{2,1}\theta_{2,1} + \beta_{2,1}\frac{\sum_{k_1,k_2} k_2 P_1(k_1,k_2)\theta_{1,1}^{k_1}\theta_{1,2}^{k_2-1}}{\sum_{k_1,k_2} k_2 P_1(k_1,k_2)} + \mu(1-\theta_{2,1})(1-\beta_{2,1}) \quad (16)$$

$$\dot{\theta}_{2,2} = -\beta_{2,2}\theta_{2,2} + \beta_{2,2}\frac{\sum_{k_1,k_2} k_2 P_2(k_1,k_2)\theta_{2,1}^{k_1}\theta_{2,2}^{k_2-1}}{\sum_{k_1,k_2} k_2 P_2(k_1,k_2)} + \mu(1-\theta_{2,2})(1-\beta_{2,2}) \quad (17)$$

With Eqs. (14)–(17) on hand, the densities associated with each distinct state can be obtained by

$$\begin{aligned} \dot{R}_1 &= \mu I_1(t), \\ S_1(t) &= \sum_{k_1,k_2}^{\infty} P_1(k_1,k_2)\theta_{1,1}^{k_1}\theta_{1,2}^{k_2}, \\ I_1(t) &= 1 - S_1(t) - R_1(t) \end{aligned} \quad (18)$$

$$\begin{aligned} \dot{R}_2 &= \mu I_2(t), \\ S_2(t) &= \sum_{k_1,k_2}^{\infty} P_2(k_1,k_2)\theta_{2,2}^{k_2}\theta_{2,1}^{k_1}, \\ I_2(t) &= 1 - S_2(t) - R_2(t) \end{aligned} \quad (19)$$

Eqs. (18) and (19) are the main theoretical results from which the theoretical results in Figs. 3–5 are calculated. Now, a critical question comes out: can our theory find out the epidemic threshold? In fact, we find that the threshold for the whole network to show epidemic outbreak can be theoretically figured out by the Jacobian matrix **J** of Eqs. (14)–(17). Particularly, the epidemic thresholds β_c^A and β_c^B can be obtained by the linear stability analysis of the trivial fixed point solution $(\theta_{1,1}, \theta_{1,2}, \theta_{2,1}, \theta_{2,2}) = (1, 1, 1, 1)$ of Eqs. (14)–(17). Without loss of generality, one can set the recovery rate $\mu = 1.0$. The Jacobian matrix **J** of Eqs. (14)–(17) at (1, 1, 1, 1) can be expressed as

$$\mathbf{J} = \begin{pmatrix} \beta_{1,1}\frac{\sum k_1(k_1-1)P_1(k_1,k_2)}{\sum k_1 P_1(k_1,k_2)} - 1 & \beta_{1,1}\frac{\sum k_1 k_2 P_1(k_1,k_2)}{\sum k_1 P_1(k_1,k_2)} & 0 & 0 \\ 0 & -1 & \beta_{1,2}\frac{\sum k_1(k_1-1)P_2(k_1,k_2)}{\sum k_1 P_2(k_1,k_2)} & \beta_{1,2}\frac{\sum k_1 k_2 P_2(k_1,k_2)}{\sum k_1 P_2(k_1,k_2)} \\ \beta_{2,1}\frac{\sum k_1 k_2 P_1(k_1,k_2)}{\sum k_2 P_1(k_1,k_2)} & \beta_{2,1}\frac{\sum k_2(k_2-1)P_1(k_1,k_2)}{\sum k_2 P_1(k_1,k_2)} & -1 & 0 \\ 0 & 0 & \beta_{2,2}\frac{\sum k_1 k_2 P_2(k_1,k_2)}{\sum k_2 P_2(k_1,k_2)} & \beta_{2,2}\frac{\sum k_2(k_2-1)P_2(k_1,k_2)}{\sum k_2 P_2(k_1,k_2)} - 1 \end{pmatrix} \quad (20)$$

For uncorrelated networks, the matrix **J** can be simplified as

$$\begin{pmatrix} \beta_{1,1}\frac{\langle k_1^2\rangle - \langle k_1\rangle}{\langle k_1\rangle} - 1 & \beta_{1,1}\frac{\langle k_1\rangle\langle k_{12}\rangle}{\langle k_1\rangle} & 0 & 0 \\ 0 & -1 & \beta_{1,2}\frac{\langle k_{12}^2\rangle}{\langle k_{12}\rangle} & \beta_{1,2}\frac{\langle k_2\rangle\langle k_{12}\rangle}{\langle k_{12}\rangle} \\ \beta_{2,1}\frac{\langle k_1\rangle\langle k_{21}\rangle}{\langle k_{21}\rangle} & \beta_{2,1}\frac{\langle k_{21}^2\rangle}{\langle k_{21}\rangle} & -1 & 0 \\ 0 & 0 & \beta_{2,2}\frac{\langle k_2\rangle\langle k_{12}\rangle}{\langle k_2\rangle} & \beta_{2,2}\frac{\langle k_2^2\rangle - \langle k_2\rangle}{\langle k_2\rangle} - 1 \end{pmatrix}$$

β_c^A and β_c^B can be obtained by seeking for the condition where the largest eigenvalue Λ of **J** changing from 0 to positive. Instead of obtaining the expression of Λ of **J**, we here numerically find the transition point of Λ from 0 to positive. The white lines in Fig. 6 show the results on SF-RR networks, i.e. the thresholds β_c^A and β_c^B, where (a) and (b) represent the case of $\langle k_{ab}\rangle = 1.0$, and (c) and (d) the case of $\langle k_{ab}\rangle = 2.0$; and (a) and (c) represent the case of $\langle \beta_{ab}\rangle = 0.1$, and (b) and (d) the case of $\langle \beta_{ab}\rangle = 0.5$. For confirmation of such a prediction, one can use the same set of parameters, and calculate numerically ρ_R of the whole SF-RR networks, which is shown in Fig. 6(a)–(d). The phase diagram of ρ_R in each panel of Fig. 6(a)–(d) can be divided into two distinct regions (whose boundaries are depicted in white lines): the healthy and endemic phases, respectively. The theoretical predictions are in good agreement with the numerical results.

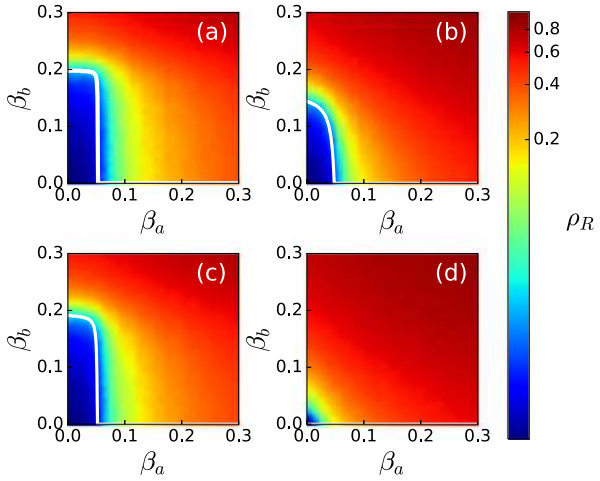

Fig. 6. Phase diagram of the final epidemic size. Dependence of ρ_R on β_a and β_b on SF-RR networks with $\langle k_{ab}\rangle = 1.0$ in (a)-(b) and $\langle k_{ab}\rangle = 2.0$ in (c)-(d). Left and right panels correspond to $\beta_{ab} = 0.1$ and $\beta_{ab} = 0.5$ respectively. The Color-coded values ρ_R are obtained from numerical simulations and the theoretical predictions (white line) are the solutions of the largest eigenvalue $\Lambda = 0$ of Jacobian matrix **J** in matrix (20). All numerical results are averaged over 1,000 independent realizations. Other parameters are $P_A(k) \sim k^{-\gamma}$, $\gamma = 2.1$, $\langle k_a\rangle = 6$, $\langle k_b\rangle = 6$, $\mu = 1$ and $N_a = N_b = 10\,000$.

When networks $\mathcal{A}$ and $\mathcal{B}$ can be treated as isolated graphs (i.e. when their coupling is particularly weak), the explicitly expression of the epidemic thresholds is obtained by setting $\Lambda = 0$, i.e. $\beta_c^A = \frac{\langle k_1\rangle}{\langle k_1^2\rangle - \langle k_1\rangle}$ and $\beta_c^B = \frac{\langle k_2\rangle}{\langle k_2^2\rangle - \langle k_2\rangle}$. When the coupling between the layers is increased, β_c^A and β_c^B decrease gradually. This result is consistent with the evidences reported in Ref. [25,58].

Fig. 7 shows the phase diagram of epidemic for different $\langle k_{ab}\rangle$ and β_{ab}, where (from top to bottom) the curves with different colors represent the epidemic threshold lines of β_c^A and β_c^B for the cases of $\beta_{ab} = 0.1, 0.3, 0.5, 0.7, 0.9, 1.0$, respectively. Panels (a) and (b) correspond to $\langle k_{ab}\rangle = 1.0$ and 2.0, respectively. In detail, each of the curves represents the boundary between the healthy

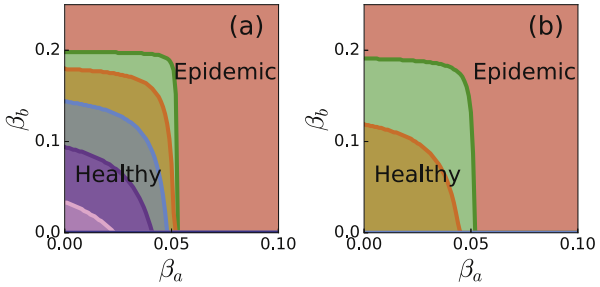

Fig. 7. Phase diagrams of the healthy and the endemic phase for (a) $\langle k_{ab}\rangle = 1.0$, and (b) $\langle k_{ab}\rangle = 2.0$. The curves indicate the boundaries of healthy and the endemic phases, where the solution are obtained by solving $\Lambda = 0$ in matrix (20). Different color curves from top to down correspond to the case of $\beta_{ab} = 0.1, 0.3, 0.5, 0.7, 0.9, 1.0$. Other parameters are $P_A(k) \sim k^{-\gamma}$, $\gamma = 2.1$, $\langle k_a\rangle = 6$, $\langle k_b\rangle = 6$, $\mu = 1$ and $N_a = N_b = 10\,000$.

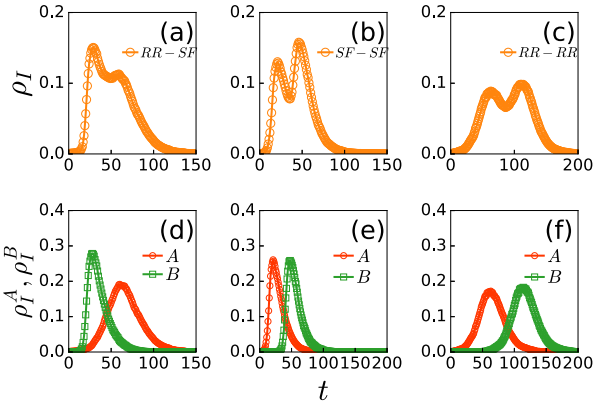

Fig. 8. The patterns of two peaks for different layer structures. (a), (b) and (c) represent the time evolutions of the infected density ρ_I in RR-SF networks, SF-SF networks, and RR-RR networks, respectively. (d), (e) and (f) show the time evolutions of ρ_I^A and ρ_I^B corresponding to (a), (b) and (c). The parameters in the left, middle, and right panels are $\langle k_{ab}\rangle = 0.01$ and $\beta_{ab} = 0.2$; $\langle k_{ab}\rangle = 0.001$ and $\beta_{ab} = 0.1$; and $\langle k_{ab}\rangle = 0.001$ and $\beta_{ab} = 0.1$, respectively. Other parameters are $P_A(k) \sim k^{-\gamma}$, $\gamma = 2.1$, $\langle k_a\rangle = 6$, $\langle k_b\rangle = 6$, $\beta_a = \beta_b = 0.05$, $\mu = 0.1$ and $N_a = N_b = 10,000$.

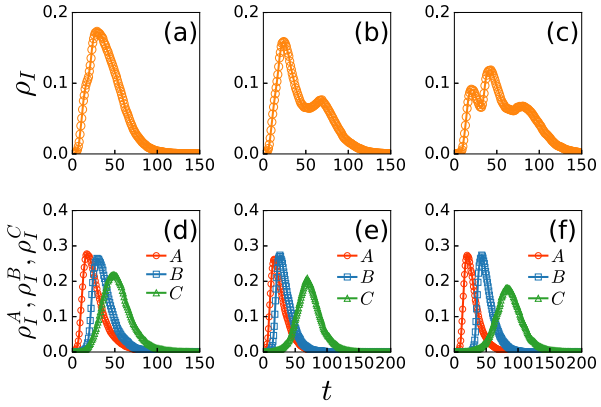

Fig. 9. Three peaks patterns in three-layered networks. Panels (a), (b) and (c) report the patterns with one peak, two peaks and three peaks of ρ_I, for a three-layered SF-SF-RR network. (d), (e) and (f) show the time evolutions of ρ_I^A, ρ_I^B and ρ_I^C corresponding to (a), (b) and (c). The parameters in the left, middle, and right panels are $\langle k_{ab}\rangle = \langle k_{ac}\rangle = \langle k_{bc}\rangle = 1$; $\langle k_{ab}\rangle = 1, \langle k_{ac}\rangle = \langle k_{bc}\rangle = 0.1$; and $\langle k_{ab}\rangle = \langle k_{bc}\rangle = 0.01, \langle k_{ac}\rangle = 0.1$, respectively. Other parameters are $P_A(k) \sim k^{-\gamma}$, $\gamma = 2.1$, $\langle k_a\rangle = \langle k_b\rangle = \langle k_c\rangle = 6$, $\beta_a = \beta_b = \beta_c = 0.05$, $\beta_{ab} = \beta_{ac} = \beta_{bc} = 0.005$, $\mu = 0.1$ and $N_a = N_b = N_c = 10,000$.

and endemic phases, and the solutions are obtained by solving the largest eigenvalue $\Lambda = 0$ of the Jacobian matrix **J**. Other parameters are set as $P_A(k) \sim k^{-\gamma}$, $\gamma = 2.1$, $\langle k_a\rangle = 6$, $\langle k_b\rangle = 6$, $\mu = 1$ and $N_a = N_b = 10,000$. Once the coupling strength is strong enough, the value of Λ is mainly determined from the contribution of the interconnection network $\mathcal{AB}$, which is similar to a pure bipartite network. Looking at Fig. 7, an interesting conclusion is that an endemic state can occur even if there are no interactions within each individual network. These results imply that, in order to control an epidemic spreading, one needs to pay more attention to the effects of the coupling strength between different regions.

6. Discussion

Let us remark that the weak coupling condition predicted by us for the occurrence of the novel epidemic pattern is actually consistent with the cases of the data of Fig. 1. As it is well known, indeed, Hong Kong in Fig. 1(a) consists of islands, and the movement of individuals between different islands is not as convenient as that within each single island, and thus the coupling between neighboring islands can be considered to be weak. At the same time, the population distribution in Hong Kong central island is significantly different from that characterizing the surrounding islands, confirming the presence of the second ingredient predicted by our theory: i.e. a difference in the heterogeneity of the layers' structures.

In Boston, a river separates the city into two parts, which (to all extent) can be considered as equivalent to two islands. The same reasoning applies to the neighboring cities of Bristol and Newcastle and the neighboring cities of Bristol and Sheffield. As Bristol and Newcastle, Newcastle and Sheffield are separated regions in the United Kingdom, and they can therefore be considered as a pair of weakly coupled networks.

Our predictions were obtained on coupled SF-RR networks, and it is legitimate to seek for generality of the two peaks pattern phenomenon, by means of investigating coupled networks with other topological structures. For this purpose, we have also studied the case of SF-SF and RR-RR networks, respectively. Very interestingly, one finds that the pattern of two peaks can be still observed by adjusting the coupling strength between the coupled layers (see Fig. 8). Although the two coupled SF networks (or the two coupled RR networks) can be considered as the case with same heterogeneity, they are produced independently and thus their network topologies are different, indicating that there exists still the effect of heterogeneity between the two coupled networks. On the other hand, extension to three-layered model was also considered, and it was found that there is a small probability to produce a pattern of three peaks (see Fig. 9). Therefore, while in principle one can expect a multi-peaks pattern to occur in a multilayered network, the majority of unusual cases (i.e. cases in which the epidemic event is not happening with a single maximum of infected density) will be characterized by just two peaks, in full consistency with the data of Fig. 1.

In summary, epidemic spreading has been well studied in the past decades but mainly focused on outbreaks corresponding to patterns with a single peak of infected density. We here reported (from real data) the evidence that also a pattern of two peaks in a single epidemic period is possible. We pointed out that such a pattern is a genuine product of a multi-layered interaction structure, and we have introduced a proper model able to fully capture the mechanisms for its occurrence. Our model, together with reproducing the classical pattern of a single peak, can generate the pattern with two peaks when coupling between the layers is weak, while the difference in heterogeneity of the layers' structures is also helpful.

Acknowledgements

Authors acknowledge the Centre for Health Protection, Department of Health, the Government of the Hong Kong Special Administrative Region, and the USA National Notifiable Diseases Surveillance System as digitized by Project Tycho for providing data. This work was partially supported by the NNSF of China under Grant Nos. 11135001, 11375066, 973 Program under Grant No. 2013CB834100.

References

[1] Pastor-Satorras R, Castellano C, Mieghem PV, Vespignani A. Epidemic processes in complex networks. Rev Mod Phys 2015;87(3):925.
[2] Barrat A, Barthelemy M, Vespignani A. Dynamical processes on complex networks. Cambridge, England: Cambridge University Press; 2008.
[3] Wang W, Tang M, Stanley HE, Braunstein LA. Unification of theoretical approaches for epidemic spreading on complex networks. Rep Prog Phys 2017;80(3):036603.
[4] Salehi M, Sharma R, Marzolla M, Magnani M, Siyari P, Montesi D. Spreading processes in multilayer networks. IEEE Trans Network Sci Eng 2015;2(2):65–83.

[5] Pastor-Satorras R, Vespignani A. Epidemic spreading in scale-free networks. Phys Rev Lett 2001;86:3200.
[6] Boguñá M, Pastor-Satorras R. Epidemic spreading in correlated complex networks. Phys Rev E 2002;66:047104.
[7] Colizza V, Pastor-Satorras R, Vespignani A. Reaction-diffusion processes and metapopulation models in heterogeneous networks. Nat Phys 2007;3:276–82.
[8] Colizza V, Vespignani A. Invasion threshold in heterogeneous metapopulation networks. Phys Rev Lett 2007;99:148701.
[9] Baronchelli A, Catanzaro M, Pastor-Satorras R. Bosonic reaction-diffusion processes on scale-free networks. Phys Rev E 2008;78:016111.
[10] Tang M, Liu L, Liu Z. Influence of dynamical condensation on epidemic spreading in scale-free networks. Phys Rev E 2009;79:016108.
[11] Vazquez A, Racz B, Lukacs A, Barabasi AL. Impact of non-Poissonian activity patterns on spreading processes. Phys Rev Lett 2007;98:158702.
[12] Meloni S, Arenas A, Moreno Y. Traffic-driven epidemic spreading in finite-size scale-free networks. Proc Natl Acad Sci USA 2009;106:16897–902.
[13] Balcan D, Colizza V, Gonçalves B, Hu H, Ramasco JJ, Vespignani A. Multiscale mobility networks and the spatial spreading of infectious diseases. Proc Natl Acad Sci USA 2009;106:21484–9.
[14] Ruan Z, Tang M, Liu Z. Epidemic spreading with information-driven vaccination. Phys Rev E 2012;86:036117.
[15] Liu S, Perra N, Karsai M, Vespignani A. Controlling contagion processes in activity driven networks. Phys Rev Lett 2014;112:118702.
[16] Tang M, Liu Z, Li B. Epidemic spreading by objective traveling. Europhys Lett 2009;87:18005.
[17] Liu Z. Effect of mobility in partially occupied complex networks. Phys Rev E 2010;81:016110.
[18] Gross T, D'Lima CJD, Blasius B. Epidemic dynamics on an adaptive network. Phys Rev Lett 2006;96(20):208701.
[19] Gross T, Kevrekidis IG. Robust oscillations in SIS epidemics on adaptive networks: Coarse graining by automated moment closure. Europhys Lett 2008;82(3):38004.
[20] Zhou J, Xiao G, Cheong SA, Fu X, Wong L, Ma S, et al. Epidemic reemergence in adaptive complex networks. Phys Rev E 2012;85(3):036107.
[21] Zhou J, Xiao G, Chen G. Link-based formalism for time evolution of adaptive networks. Phys Rev E 2013;88(3):032808.
[22] Marceau V, Noël PA, Hébert-Dufresne L, Allard A, Dubé LJ. Adaptive networks: Coevolution of disease and topology. Phys Rev E 2010;82(3):036116.
[23] Boccaletti S, Bianconi G, Criado R, del Genio CI, Gómez-Gardeñes J, Romance M, et al. The structure and dynamics of multilayer networks. Phys Rep 2014;544:1.
[24] Feng L, Monterola CP, Hu Y. The simplified self-consistent probabilities method for percolation and its application to interdependent networks. New J Phys 2015;17(6):063025.
[25] Sahneh FD, Scoglio C, Chowdhury FN. Effect of coupling on the epidemic threshold in interconnected complex networks: A spectral analysis. In 2013 American control conference (pp. 2307–2312). IEEE; 2013.
[26] Wang H, Li Q, D'Agostino G, Havlin S, Stanley HE, Mieghem PV. Effect of the interconnected network structure on the epidemic threshold. Phys Rev E 2013;88(2):022801.
[27] Yagan O, Qian D, Zhang J, Cochran D. Conjoining speeds up information diffusion in overlaying social-physical networks. IEEE J Sel Areas Commun 2013;31(6):1038–48.
[28] Newman MEJ. Threshold effects for two pathogens spreading on a network. Phys Rev Lett 2005;95(10):108701.
[29] Marceau V, Noël PA, Hébert-Dufresne L, Allard A, Dubé LJ. Modeling the dynamical interaction between epidemics on overlay networks. Phys Rev E 2011;84:026105.
[30] Buono C, Braunstein LA. Immunization strategy for epidemic spreading on multilayer networks. Europhy Lett 2015;109(2):26001.
[31] Buono C, Alvarez-Zuzek LG, Macri PA, Braunstein LA. Epidemics in partially overlapped multiplex networks. PloS One 2014;9(3):e92200.
[32] Zhao Y, Zheng M, Liu Z. A unified framework of mutual influence between two pathogens in multiplex networks. Chaos 2014;24:043129.
[33] Holme P, Saramäki J. Temporal networks. Phys Rep 2012;519:97–125.
[34] Perra N, Goncalves B, Pastor-Satorras R, Vespignani A. Activity driven modeling of time varying networks. Sci Rep 2012;2:469.
[35] Grenfell BT, Bjurnstad ON, Kappey J. Travelling waves and spatial hierarchies in measles epidemics. Nature 2001;41:716.
[36] Heesterbeek H, Anderson RM, Andreasen VI, et al. Modeling infectious disease dynamics in the complex landscape of global health. Science 2015;347:aaa4339.
[37] Watts DJ, Muhamad R, Medina DC, Dodds PS. Multiscale, resurgent epidemics in a hierarchical metapopulation model. Proc Natl Acad Sci USA 2005;102:11157–62.
[38] Balcana D, Colizzac V, Goncalves B, Hu H, Ramasco JJ, Vespignania A. Multiscale mobility networks and the spatial spreading of infectious diseases. Proc Natl Acad Sci USA 2009;106:21484–9.
[39] Department of Health, Hong Kong. Weekly consultation rates of influenza-like illness data. http://www.chp.gov.hk/en/sentinel/26/44/292.html. Date of access: 15/06/2014.
[40] Zheng M, Wang C, Zhou J, Zhao M, Guan S, Zou Y, et al. Non-periodic outbreaks of recurrent epidemics and its network modelling. Sci Rep 2015;5:16010.
[41] The USA national notifiable diseases surveillance system weekly measles infective cases. http://www.tycho.pitt.edu/. Date of access: 04/08/2016.
[42] Scarpino SV, Allard A, Hébert-Dufresne L. The effect of a prudent adaptive behaviour on disease transmission. Nat Phys 2016;3832:1745–2481.
[43] http://ms.mcmaster.ca/~bolker/measdata.html.
[44] Catanzaro M, Boguñá M, Pastor-Satorras R. Generation of uncorrelated random scale-free networks. Phys Rev E 2005;71:027103.
[45] Ruciński A, Wormald NC. Random graph processes with degree restrictions. Comb Probab Comput 1992;1(2):169–80.
[46] Barthélemy M, Barrat A, Pastor-Satorras R, Vespignani A. Velocity and hierarchical spread of epidemic outbreaks in scale-free networks. Phys Rev Lett 2004;92(17):178701.
[47] Volz E. SIR dynamics in random networks with heterogeneous connectivity. J Math Biol 2008;56(3):293–310.
[48] Miller JC. A note on a paper by Erik Volz: SIR dynamics in random networks. J Math Biol 2011;62(3):349–58.
[49] Shu P, Wang W, Tang M, Zhao P, Zhang YC. Recovery rate affects the effective epidemic threshold with synchronous updating. Chaos 2016;26(6):063108.
[50] Miller JC, Slim AC, Volz EM. Edge-based compartmental modelling for infectious disease spread. J R Soc Interface 2012;9(70):890–906.
[51] Volz EM, Miller JC, Galvani A, Meyers LA. Effects of heterogeneous and clustered contact patterns on infectious disease dynamics. PLoS Comput Biol 2011;7(6):e1002042.
[52] Valdez LD, Macri PA, Braunstein LA. Temporal percolation of the susceptible network in an epidemic spreading. PLoS One 2012;7(9):e44188.
[53] Miller JC, Volz EM. Incorporating disease and population structure into models of SIR disease in contact networks. PloS One 2013;8(8):e69162.
[54] Miller JC. Epidemics on networks with large initial conditions or changing structure. PloS One 2014;9(7):e101421.
[55] Miller JC. Cocirculation of infectious diseases on networks. Phys Rev E 2013;87(6):060801.
[56] Wang W, Tang M, Shu P, Wang Z. Dynamics of social contagions with heterogeneous adoption thresholds: Crossover phenomena in phase transition. New J Phys 2016;18(1):013029.
[57] Decreusefond L, Dhersin JS, Moyal P, Tran VC. Large graph limit for an SIR process in random network with heterogeneous connectivity. Ann Appl Probab 2012;22(2):541–75.
[58] Saumell-Mendiola A, Serrano MA, Boguñá M. Epidemic spreading on interconnected networks. Phys Rev E 2012;86:026106.